MISR radiometric uncertainty analyses and their utilization within geophysical retrievals

C. J. Bruegge, N. L. Chrien, D. J. Diner, R. A. Kahn and J. V. Martonchik

Abstract. The Multi-angle Imaging SpectroRadiometer (MISR) is to be launched with the Earth Observing System EOS-AM1 spacecraft in 1999. Demanding specifications include a requirement that the instrument be calibrated, and placed on an accurate radiometric scale, to within 3 % (1σ) uncertainty, for incident radiances near the upper end of a camera's dynamic range. Contributing factors to the uncertainty in radiance measurements include signal-to-noise ratio, goodness of fit of the calibration data to a quadratic equation, and quality of the experimental conditions (i.e. range and number of radiometric levels used to provide the calibration). These sources, as they are identified, are flagged as contributing to the absolute, relative band-to-band, relative camera-to-camera, or relative pixel-to-pixel radiance uncertainties. This paper summarizes the products and results from the uncertainty analysis of radiometric calibrations for the MISR. It also provides an example of a geophysical product retrieval that makes use of these data.

1. Introduction

The Multi-angle Imaging SpectroRadiometer (MISR) has been designed and built by the Jet Propulsion Laboratory (JPL) for a launch in 1999 as one of five instruments on the first Earth Observing System platform (EOS-AM1). Details of the instrument design and scientific objectives are given in [1]. The instrument consists of nine cameras, each with a unique view angle to Earth. Each camera makes use of four charge-coupled-device (CCD) line arrays, filtered to spectral bands centred at 446 nm, 558 nm, 672 nm and 866 nm (as determined from a solar-weighted, in-band moments analysis). These bands are termed Bands 1 to 4, or Blue, Green, Red and Near-Infrared (NIR), respectively. There exist 1504 active elements per line array, with thirty-six channels (nine cameras and four spectral bands) for the instrument. The contents of the CCD serial registers, termed "overclock pixels", are sampled following the active pixel read. They provide a measure of the dynamic video offset bias. The final output of the camera is provided in the form of 14-bit digital numbers (DN).

Each of the nine flight cameras was built and tested in series. Verification of boresight alignment, focus and effective focal length was followed by radiometric and spectral calibration, and polarization-response verification. Testing was done under vacuum conditions, at temperatures predicted for the flight environment. The CCD focal planes are actively controlled at $-5\,^{\circ}$C.

During radiometric calibration the relationship between an incident radiance field and a camera digital output is measured. The radiometric scale is established pre-flight (and in-flight) for the MISR using detector standards. For pre-flight testing two types of detector standard are used [2]. A QED-200 (made of United Detector Technology inversion-layer diodes) is used to measure sphere output for MISR Bands 1 and 2; a QED-150 (made of Hamamatsu p-on-n photodiodes) is used for Bands 3 and 4. (For the flight calibration, custom devices have been built, in order to minimize the size of the photodiodes [3].) Each standard is made of three silicon photodiodes, mounted in a light-trap configuration so as to collect the light reflected at each air/detector interface. Each photodiode is designed to have 100 % internal quantum efficiency for the wavelength region at which it is operated. These standards are used with filters of the same spectral bandpass design as for the flight cameras, and with a known field-of-view, established with a high-precision aperture tube. Traceability to the International System of Units (SI) is established through the measurement protocols of current, apertures and aperture distances. The JPL maintains working standards of voltage, resistance and length which are traceable to the National Institute of Standards and Technology (NIST) or other international standards that are recognized by the NIST. The filter transmittance

C. J. Bruegge, N. L. Chrien, D. J. Diner, R. A. Kahn and J. V. Martonchik: Jet Propulsion Laboratory, California Institute of Technology, 4800 Oak Grove Drive, Pasadena, CA 91109, USA.

for each of the standards is measured with a dual-beam spectrometer, with an uncertainty of less than 0.5 %. The internal quantum efficiency and reflectance loss of the standards are assumed to be unity and zero, respectively, with an uncertainty of 0.1 % as per the manufacturer's specification. The accuracy of these trap devices has been well established in the literature [4, 5].

In addition to these standards, a flat-field source is required for radiometric calibration. For pre-flight calibration we use an integrating sphere 1.6 m (65″) in diameter that has a 76 cm × 23 cm (30″ × 9″) exit port and a 30 cm (12″) external sphere with a variable aperture at the entrance port to the large sphere. The sphere is run through a sequence of lamp-on settings, allowing digital data to be collected at twelve radiometric levels, evenly spaced within the dynamic range of each spectral channel. Operationally, the sphere is initially turned on to its maximum intensity setting and allowed to warm up for 20 min. After data acquisition, the remaining output levels are achieved quickly since all bulb transitions are from on to off. Prior to each camera calibration, the output radiance of the sphere is established at each of its pre-programmed output levels using the standards, which view the sphere through the window of the vacuum chamber. The camera is then inserted into the thermal vacuum chamber, also viewing the sphere through the window. Sixty-four measurements are made at each level to allow noise analysis, and the procedure for the full-on to lowest-output-level cycle is repeated three times to guarantee that the necessary data are acquired and as a consistency check on the calibration. A broadband photodiode, mounted so as to view the back wall of the sphere, is used to verify sphere stability during a particular data-acquisition run.

With these data, the coefficients in the calibration equation can be determined for each pixel of each spectral channel. For the MISR this is done using a quadratic calibration equation. This functional form produces lower residuals than a linear fit, significant at the lower end of the response range. The relationship used in both calibration and Level 1 radiance retrieval is

$$G_2(\mathcal{L}^{\mathrm{std}})^2 + G_1\mathcal{L}^{\mathrm{std}} + G_0 = D - D_0, \qquad (1)$$

where

$\mathcal{L}^{\mathrm{std}}$ [W m^{-2} sr^{-2} μm^{-1}] is the incident radiance weighted by the spectral-response profile. The profile used is termed the "standardized response function", and is an average of the profiles measured for a particular spectral band,

D is the camera DN output,

G_2, G_2 and G_0 are best-fit parameters to the measured radiative transfer curve, and

D_0 is the DN output of the video offset signal, unique for each line of data, and measured by the overclock readout for that line.

For the MISR cameras, the CCD response is nearly linear and the G_0 and G_2 $(\mathcal{L}^{\mathrm{std}})^2$ terms are small relative to the $G_1\mathcal{L}^{\mathrm{std}}$ term. G_0 typically ranges from −5 DN to 10 DN; G_2 is typically 0.001 DN/(W m^{-2} sr^{-2} μm^{-1})^2. To first order, the camera response is given by the G_1 coefficient, which ranges from about 20 DN to 40 DN/(W m^{-1} sr^{-1} μm^{-1}) (see [2]).

In addition to producing radiometric coefficients, the calibration team also provides uncertainties for the radiance measurements. These include absolute radiance uncertainty, and band-to-band relative, camera-to-camera relative, and pixel-to-pixel relative uncertainties. Both the coefficients and radiance uncertainties are compiled in a data file called the Ancillary Radiometric Product (ARP) [6]. The MISR geophysical retrieval algorithms (which produce aerosol, land-surface, and cloud products) make use of these uncertainties during standard processing [7, 8]. Because MISR uncertainty values are used in science-product generation, their computation must be well-documented and reviewed. This paper describes the uncertainty analysis that was performed for MISR pre-flight radiometric calibration. In order to reduce systematic errors, the MISR makes use of multiple calibration approaches. In a subsequent section, a description is given of how coefficients are combined from the various processing pathways. The final section contains an example of an algorithm which makes use of the radiometric uncertainty values.

2. Uncertainty analysis

2.1 Mathematical development

We begin this section by defining the terms absolute and relative (band-to-band, camera-to-camera, and pixel-to-pixel) uncertainties, as used by the MISR community. The term "relative uncertainty" is used to denote the uncertainty in the ratio of two observables. For clarity we do not use the term "relative uncertainty" to refer to the absolute uncertainty normalized by the value itself (i.e. $\delta L/L$). Although this is commonly done in the metrology community, our approach does not conflict with commonly referenced guidelines (see [9]). Care has been taken to refer to error as a departure of our measurement from the true value (an unknown), and uncertainty as our estimation of this error. Also, it is appropriate to emphasize that all radiometric uncertainties reported in the MISR are given at the 1σ confidence level. Sixty-eight percent of the probability distribution is encompassed by the uncertainty estimate. Finally, it is noted that the uncertainties, when expressed in units of the parameter, are denoted using the symbol σ, whereas when expressed as a percentage, the symbol ε is utilized. With this introduction we provide the following MISR definitions:

Absolute uncertainty, σ_{abs}. The estimation of the departure of a radiance measurement, L_{mea}, from the true value, L_{true}: $\sigma_{\mathrm{abs}} = |L_{\mathrm{mea}} - L_{\mathrm{true}}|$.

Fractional absolute uncertainty, $\sigma_{\mathrm{abs}}/L_{\mathrm{true}}$. The estimation of the deviation of a measurement from truth, normalized by the true value.

Percentage absolute uncertainty, $\varepsilon_{\rm abs}$. The estimation of the deviation of a measurement from truth, normalized by the true value and expressed as a percentage: $\varepsilon_{\rm abs} = (\sigma_{\rm abs} \times 100)/L_{\rm true}$. (The absolute uncertainties reported to the MISR ARP file are percentage uncertainties.)

Relative uncertainty, $\sigma_{\rm rel}$. The estimation of the deviation in the ratio of two measurements from the true ratio. To describe this mathematically we let the ratio of measurements L_1 and L_2 be denoted $R_{\rm rel}$, and the ratio of the true values $L_{\rm true,\,1}$ and $L_{\rm true,\,2}$ be denoted $R_{\rm true}$. We then have $\sigma_{\rm rel} = |R_{\rm rel} - R_{\rm true}|$. Specific relative uncertainties of interest to the MISR are:

- *Percentage band-to-band relative uncertainty*, $\varepsilon_{\rm band}$. The uncertainty in the ratio of radiances measured by two separate bands within a given camera, expressed as a percentage of the true ratio;
- *Percentage camera-to-camera relative uncertainty*, $\varepsilon_{\rm cam}$. The uncertainty in the ratio of radiances measured by two separate cameras of a common band, expressed in units of a percentage of the true ratio; and
- *Percentage pixel-to-pixel relative uncertainty*, $\varepsilon_{\rm pix}$. The uncertainty in the ratio of radiances measured by two separate pixels within a given MISR channel, expressed as a percentage of the true ratio.

Fractional relative uncertainty, $\sigma_{\rm rel}/R_{\rm true}$. The estimation of the deviation of the ratio of two measurements from the true ratio, normalized by the true ratio.

Percentage relative uncertainty, $\varepsilon_{\rm rel}$. The estimation of the difference of the ratio of two measurements from the true ratio, normalized by the true ratio and expressed as a percentage: $\varepsilon_{\rm rel} = (\sigma_{\rm rel} \times 100)/R_{\rm true}$.

Error sources. These are the contributors which may lead to a finite uncertainty in the measured incident radiance. That is, each absolute or relative uncertainty is computed by taking the root-sum-square (RSS) of the radiance uncertainty estimates identified for each error source. It is understood that the term "error source" is a misnomer, in that a parameter may represent an approach, rather than an error. For example, one cannot say that one functional form of the calibration equation, used to express the measured light-response curve, leads to an error, as compared with another. Rather, each represents an approach which provides the required radiance-retrieval to within some stated uncertainty.

Systematic errors. Those error sources which result in a static offset between the measured and true value of a parameter, or a static offset in the ratio of two measured parameters, as compared with the true value of that parameter.

Random errors. Those error sources which result in a random offset between consecutive measured and true values. The contribution of these errors diminishes by the square root of the number of averaged measurements. Fractional random error is the inverse of the signal-to-noise ratio.

Although we have taken care to make these distinctions, we often refer loosely to absolute or relative uncertainties when we may be referring to their fractional or percentage equivalent. The text will clarify which is intended, if such a distinction is important to the discussion.

A mathematical development of the uncertainty algorithm further helps to define what is meant by absolute and relative uncertainty, as well as to define how these parameters are used to estimate the uncertainty in radiance ratio for a particular set of observations. Let the radiance retrieved from a given camera be expressed as

$$L = L_{\rm true}\prod(1 + s_i) \approx L_{\rm true}(1 + \sum s_i), \qquad (2)$$

where the $(1 + s_i)$ factors are due to independent error sources distinguished by index i. We believe that the errors combine by the multiplicative model shown by the centre relationship. Further, as each of the errors is small, the approximation given on the right-hand side of (2) can be made. That is, the product is approximated by the sum of the error values. In practice the error values, s_i, are not known, but can be represented by a Gaussian probability distribution of zero mean and a defined $1\,\sigma$ standard deviation. We thus modify the approximation to acknowledge that only the probabilities in each error term are known. Specifically, we substitute the sum of the error terms with an RSS. We also change notation, replacing the unknown error values with their estimated probability distribution half-widths, ε_i. The division by 100 arises because we have defined ε as a percentage. Thus,

$$\langle L \rangle = L_{\rm true}(1 \pm \varepsilon_{\rm abs}/100), \qquad (3)$$

where

$$\varepsilon_{\rm abs} = \sqrt{\sum \varepsilon^2_{{\rm abs},\,i}}, \qquad (4)$$

and where $\varepsilon_{\rm abs}$ is referred to as the percentage absolute radiometric uncertainty in the estimated parameter, L.

Now consider the relative camera-to-camera radiance, given by the expression $R_{\rm cam} = L_1/L_2$, where L_1 and L_2 are the radiances measured from two channels of different cameras but within the same spectral band. For this case we take the right-hand-side expansion of (2) and write

$$\begin{aligned} R_{\rm cam} = \frac{L_1}{L_2} &\approx \frac{L_{1,\,\rm true}(1 + \sum s_{1,i})}{L_{2,\,\rm true}(1 + \sum s_{2,i})} \\ &\approx R_{\rm true}(1 + \sum s_{1,i})(1 - \sum s_{2,i}) \\ &\approx R_{\rm true}[1 + \sum (s_{1,i} - s_{2,i})]. \end{aligned} \qquad (5)$$

We first note that any error value that is known to contribute equally to the uncertainty in L_1 and L_2 cancels (i.e. systematic errors where $s_{1,i} = s_{2,i}$). Next, using the same argument as above, we assume that the $s_{1,i}$ and $s_{2,i}$ values are all independent, and our estimate of R is based on our estimate of the probabilities of ε. For this reason we substitute the difference in (5) with the RSS of the camera-relative uncertainties. Those which are camera-dependent are so labelled and denoted $\varepsilon_{\mathrm{cam},1,i}$ for uncertainties related to camera 1, and $\varepsilon_{\mathrm{cam},2,i}$ for uncertainties related to camera 2. We conclude:

$$\langle R_{\mathrm{cam}} \rangle = R_{\mathrm{true}}(1 \pm \varepsilon_{\mathrm{cam}}/100), \tag{6}$$

where

$$\varepsilon_{\mathrm{cam}} = \sqrt{\sum \varepsilon^2_{\mathrm{cam},1,i} + \sum \varepsilon^2_{\mathrm{cam},2,i}}, \tag{7}$$

and $\varepsilon_{\mathrm{cam}}$ is the percentage camera-to-camera relative uncertainty. The uncertainty in the ratio of radiances is found to be represented by the RSS of the camera-relative uncertainties for each of the two cameras. This uncertainty [(6) and (7)] is less than the absolute uncertainty in radiance [(3) and (4)] only if the camera-relative uncertainties are small compared with the other terms.

Similar expressions can be derived for the ratio of radiances from different bands, or the ratio of radiances from different pixels. In these cases, the appropriate error is written as the RSS of the error-source uncertainties that are band-relative, or pixel-relative (that is, where the error source is a random error for the measurement of radiance in one band as compared with another, or one pixel as compared with another).

2.2 Pre-flight calibration summary

Tables 1a and 1b detail one error source: that due to the determination of radiance from the pre-flight laboratory standards. This uncertainty is discussed in the Introduction, as the standards are key to providing traceability to SI units. The uncertainty in the internal quantum efficiency (QE) of the devices is of the order of 0.2 %, as determined by a comparison of the response of several such standards. The largest error source is the uncertainty of filter transmittance, 0.5 %. As is the MISR convention, all uncertainties are specified at a $1\,\sigma$ confidence level unless otherwise denoted.

Table 2 provides a list of all error sources that apply to radiometric calibration. These uncertainties are reported at two incidence-illumination levels, $\rho_{\mathrm{eq}} = 1.0$ and $\rho_{\mathrm{eq}} = 0.05$. (The equivalent reflectance, ρ_{eq}, is defined as the incident radiance multiplied by π and divided by the band-weighted exo-atmospheric solar irradiance [2].) The last four columns flag each of the error sources according to the types of uncertainty involved therein (absolute, $\varepsilon_{\mathrm{abs},i}$; camera-relative, $\varepsilon_{\mathrm{cam},c,i}$; band-relative, $\varepsilon_{\mathrm{band},c,i}$; or pixel-relative, $\varepsilon_{\mathrm{pix},i}$). The index c specifies the channel (i.e. an integer from 1 to 36); the index i represents the i-th error source. In the pre-flight calibration experiment, all radiometric error sources were measured or modelled to be independent of channel. For this reason, we have not presented the error sources for each channel – they are identical. (The ARP allows for channel-dependent errors, and thus maintains a more general error table. In particular, signal-to-noise ratio (SNR) is specified on a per-channel basis).

The parameters included in Table 2 are:

Diode radiance uncertainty. The MISR makes use of commercial light-trapped, high-QE photodiodes as its radiometric standards. These are used to establish the integrating-sphere output at the four

Table 1a. Laboratory-standard radiance error sources, Blue and Red Bands, QED-200 (Blue) UDT inversion layer diodes.

Parameter	Percentage uncertainty	Method of estimation
Internal QE > 0.998 (400 nm to 700 nm)	0.2	Comparison of different diode types
Reflection loss < 20 % per diode	0.03	JPL and vendor tests
Linearity > 99.8 %	0.25	Vendor test and JPL analysis
Signal-to-noise ratio 1000	0.1	Test and analysis
Spectral bandwidth ± 0.1 nm	0.3	Cary measurements and analysis
Filter transmission ≈ 60 %	0.5	Cary measurements and analysis
Out-of-band transmission	0.1	Cary measurements and analysis
Étendue 3.55×10^{-4} cm^2 sr	0.21	Tolerancing and inspection of fabricated parts and alignment
RSS total	0.72	

Table 1b. Laboratory-standard radiance error sources, Green and Near-Infrared Bands, QED-150 (Red) Hamamatsu p-on-n diodes.

Parameter	Percentage uncertainty	Method of estimation
Internal QE > 0.996 (600 nm to 950 nm)	0.2	Comparison of different diode types
Reflection loss < 30 % per diode	0.24	JPL and vendor tests
Linearity > 99.9 %	0.25	Vendor test and JPL analysis
Signal-to-noise ratio 2000	0.05	Test and analysis
Spectral bandwidth ± 0.1 nm	0.4	Cary measurements and analysis
Filter transmission ≈ 60 %	0.5	Cary measurements and analysis
Out-of-band transmission	0.1	Cary measurements and analysis
Étendue 3.55×10^{-4} cm^2 sr	0.21	Tolerancing and inspection of fabricated parts and alignment
RSS total	0.79	

Table 2. Pre-flight radiometric error sources.

Parameter	Percentage uncertainty at $\rho_{eq} = 1.0$	Percentage uncertainty at $\rho_{eq} = 0.05$	Uncertainty type: Absolute, ε_{abs}	Camera-relative, ε_{cam}	Band-relative, ε_{band}	Pixel-relative, ε_{pix}
Diode radiance uncertainty: internal QE, linearity, SNR, filter transmittance	0.8	0.8	=			
Diode radiance uncertainty: filter transmittance only	0.5	0.5			=	
Diode to camera out-of-band correction	1.0	1.0	=			
Sphere non-uniformity correction	0.2	0.2	=	=		=
Sphere temporal stability	1.0	1.0	=	=		
Sphere-colour temperature stability	0.1	0.1			=	
Calibration-equation fit	0.02	0.02	=			
Selection of radiometric levels	0.1	0.1	=			
SNR	0.1	0.5	=	=	=	=

MISR spectral bands. The term considered in row 2 is detailed in Table 1.

Filter transmittance. This is one component of the radiance uncertainty. It alone contributes to the band-to-band relative uncertainty.

Correction for diode-to-camera out-of-band differences. Although the filters used for the cameras and laboratory photodiode standards are of the same design, the final as-built responses are slightly different. These differences are characterized, and corrections are made with these measurements. The dominant error in the correction is the use of a single representative spectral-response function for each pixel.

Sphere non-uniformity. The sphere has been measured to be 3 % different at the field-edges, as compared with smaller-view angles. This output deviation with view angle is slowly varying, and thus only a few measurement points are needed to characterize it. This determination is used to adjust the incident radiances over the field-of-view of a given camera. The uncertainty listed is the scatter in non-uniformity measurements for the different camera calibrations.

Sphere stability. Stability-monitor readings are recorded during calibration of both the sphere and the cameras. Sphere stability is 0.3 % after the specified warm-up period. A larger instability is noted in the monitor readings in comparing sphere-calibration runs (laboratory standards viewing the sphere), and the camera calibrations. Here the bulbs have been cycled on and off many times. As no correction is made for either of these drifts, the combined uncertainty is 1 %.

Sphere-colour temperature stability. Should there be a drift in the sphere-bulb temperature, there would be a corresponding change in the sphere output radiance for one band relative to another. The magnitude of this error has not been characterized, except to assume that it is much less than the overall sphere stability reported above. It is used in the band-to-band relative uncertainty determination.

Calibration-equation fit. This error has been determined by comparing the residuals between the measured DN and those predicted from the calibration coefficients.

Selection of radiometric levels. The non-linear term of the Fidelity Interval Analysis [10] is used to estimate the error resulting from the selection of test radiometric levels, as compared with the dynamic range of a camera.

Signal-to-noise ratio (SNR). The SNR reported here is the mean DN output divided by its standard deviation, as acquired when a series of observations are made of a flat-field source. The source is assumed to be stable during the time of data acquisition (a 2 s interval).

The root-sum-square of the first column provides the absolute uncertainty, summarized in Table 3. As in (7), the RSS of the uncertainties contained within the column labelled relative, multiplied by $\sqrt{2}$, gives the relative uncertainty. All these are summarized in Table 3, assuming that the two observables in the ratio have the same radiance value.

The only calibration which did not meet its specification was the camera-relative calibration at $\rho_{eq} = 1.0$. The uncertainty for this case is dominated

Table 3. Pre-flight cumulative radiometric uncertainties.

Radiometric uncertainty	Actual: Percentage uncertainty at $\rho_{eq} = 1.0$	Actual: Percentage uncertainty at $\rho_{eq} = 0.05$	Requirement: Percentage uncertainty at $\rho_{eq} = 1.0$	Requirement: Percentage uncertainty at $\rho_{eq} = 0.05$
Absolute, ε_{abs}/%	1.6	1.7	3	6
Camera-to camera relative, ε_{cam}/%	1.4	1.6	1	2
Band-to-band relative, ε_{band}/%	0.7	1	1	2
Pixel-to-pixel relative, ε_{pix}/%	0.3	0.7	0.5	1

by the temporal stability of the sphere (change in output between the time of sphere calibration and that of camera-test-data acquisition). Clearly, a more accurate approach would have been to use a radiance-stabilized sphere, or one monitored by temperature-stabilized, filtered, monitoring photodiodes. We expect the in-flight measured uncertainties to be closer to the requirement, as better methods will be available from orbit. For example, multiple cameras will view the calibration targets simultaneously. Additionally, the AirMISR camera, which flies on an ER-2 aircraft, can provide accurate camera-relative calibrations [11], and histogram equalization can provide accurate pixel-relative calibrations. The latter experiment collects images over a large number of Earth scenes. These are then binned, for each pixel, into counts for a given DN range. For pixels in close enough proximity that atmospheric differences, due to their view-angle differences, are negligible, a relative calibration is obtained by computing the pixel-dependent scaler that would allow all histograms to be superimposed.

2.3 Pixel averaging

The ARP contains the absolute and relative uncertainties $\varepsilon_{\mathrm{abs}}$, $\varepsilon_{\mathrm{cam}}$, $\varepsilon_{\mathrm{band}}$ and $\varepsilon_{\mathrm{pix}}$, as computed by the above-described algorithms. These are given at fifteen specific equivalent-reflectance levels defined by the ARP, and for each camera and band. Since the MISR instrument operates in Global Mode for much of an orbit, and as this mode transmits pixel-averaged data for many channels, the uncertainty parameters may overestimate the radiance uncertainties because SNR is a random source of uncertainty which increases with pixel averaging. In order to allow the processing algorithms to utilize the best estimate of radiance uncertainties, the RSS of the uncertainties from all error sources, excluding SNR, is provided. These parameters are denoted $\varepsilon_{\mathrm{abs\_sys}}$, $\varepsilon_{\mathrm{cam\_sys}}$, $\varepsilon_{\mathrm{band\_sys}}$ and $\varepsilon_{\mathrm{pix\_sys}}$, where the suffix sys denotes systematic error. They are also given for fifteen equivalent-reflectance levels and thirty-six instrument channels. To compute these uncertainty parameters from the pre-flight data, the RSS values of the first eight parameters from Table 2 are root-sum-squared (if flagged for the particular absolute or relative uncertainty parameter). From Table 2 we would obtain the values 1.6, 1.0, 0.5 and 0.2, respectively, for these averaging-mode-independent parameters. The algorithms can then include the SNR component of the radiance error using the value appropriate for the number of pixels averaged, $\mathrm{SNR_{am}}$. Here the notation $\mathrm{SNR_{am}}$ is used to indicate that the SNR depends on the "averaging mode", or the number of pixels averaged. Thus,

$$\varepsilon_{\mathrm{abs}} = \sqrt{\varepsilon^2_{\mathrm{abs\_sys}} + (100/\,\mathrm{SNR_{am}})^2}. \tag{8}$$

When the parameters $\varepsilon_{\mathrm{cam\_sys}}$ and $\mathrm{SNR_{am}}$ have values that are identical for two channels, we find the camera-relative uncertainty from

$$\varepsilon_{\mathrm{cam}} = \sqrt{2} \cdot \sqrt{\varepsilon^2_{\mathrm{cam\_sys}} + (100/\,\mathrm{SNR_{am}})^2}. \tag{9}$$

To illustrate how pixel averaging affects the radiometric uncertainties, Figure 1 shows how photon, quantization and "other electronic" noise components (N_{p}, N_{q}, N_{o}, respectively) vary as a function of the number of pixels averaged. In the model [2] quantization noise, unlike the other components, is not reduced with averaging mode. For this reason, there is little change in the total noise, N_{t}, as one averages more than 4×4 pixels. Table 4 makes use of $\mathrm{SNR_{am}}$ as computed from this model. The uncertainties do not change by more than 0.1 % in going from the 4×4 to 16×16 pixel averaging case, for equivalent-reflectance

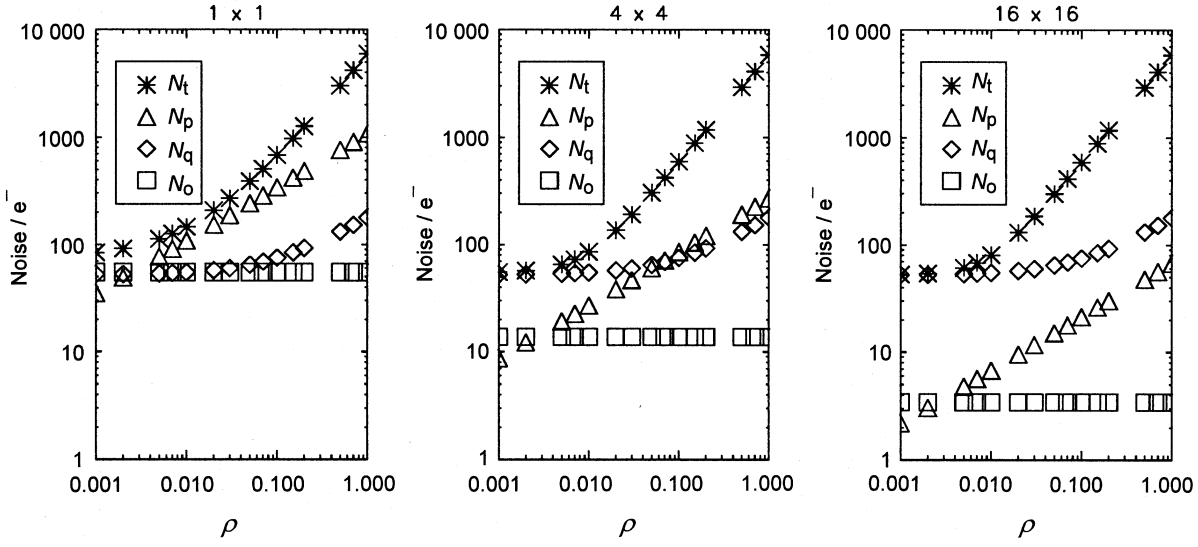

Figure 1. Photon, quantization and other noise components (N_{p}, N_{q} and N_{o}, respectively), and total noise N_{t}, as a function of 1×1, 4×4 and 16×16 pixel averaging. Values for Band 3 with camera Af, on-axis.

Table 4. Camera-relative uncertainty reduction due to pixel averaging.

Equivalent reflectance, ρ_{eq}	Percentage uncertainty from $\mathrm{SNR_{am}}$ error source [%] versus averaging mode			Combined percentage camera-relative uncertainty [%] versus averaging mode		
	1×1	4×4	16×16	1×1	4×4	16×16
0.001	7.5	4.9	4.7	10.6	7.1	6.8
0.002	4.0	2.5	2.4	5.9	3.8	3.6
0.005	1.9	1.0	1.0	3.1	2.1	2.0
0.007	1.5	0.8	0.7	2.6	1.8	1.8
0.01	1.2	0.6	0.5	2.2	1.6	1.6
0.02	0.8	0.3	0.3	1.8	1.5	1.5
0.03	0.6	0.2	0.2	1.7	1.5	1.5
0.05	0.5	0.2	0.1	1.6	1.5	1.5
0.07	0.4	0.1	0.1	1.6	1.5	1.4
0.1	0.3	0.1	0.1	1.5	1.4	1.4
0.15	0.3	0.1	0.1	1.5	1.4	1.4
0.2	0.2	0.1	0.0	1.5	1.4	1.4
0.5	0.1	0.0	0.0	1.5	1.4	1.4
0.7	0.1	0.0	0.0	1.5	1.4	1.4
1.0	0.1	0.0	0.0	1.4	1.4	1.4

inputs greater than 0.005 (i.e. 0.5 %). For this reason, it is sufficient to extract $\mathrm{SNR_{am}}$ from the 1×1, 1×4, 2×2, or 4×4 cases in the ARP.

3. In-flight calibration

3.1 Combining multiple methodologies

For the in-flight programme, a complete error analysis will be undertaken for each calibration methodology. These methodologies include calibrations using data acquired from the On-Board Calibrator (OBC), reflectance-based vicarious calibrations, AirMISR underflights, and histogram equalization. Our plans call for all data to be used, weighted by their uncertainties.

The error budgets for the various methodologies are given in Table 5. The error sources for OBC include diode radiance accuracy (2 % radiance uncertainty, including degradation during mission life), diffuse-panel spatial non-uniformity (0.2 %), panel relative bidirectional reflectance factor (BRF) (2 %), panel flatness (0.01 %), calibration-equation fit (0.02 %), radiometric levels (0.01 %), and SNR.

Table 5. In-flight radiometric error budgets.

Methodology	Percentage uncertainty at $\rho_{\mathrm{eq}} = 1.0$			
	Absolute	Camera-to-camera	Band-to-band	Pixel-to-pixel
OBC	2.8	2.8	0.8	0.4
Reflectance-based vicarious	5.0 (D camera); 3.0 (nadir)			
AirMISR		1		
Histogram equalization				0.5
Requirement	3	1	1	0.5

Not all methods can provide a determination of both absolute and relative values of the gain coefficients. As the reflectance-based vicarious technique measures surface reflectance and atmospheric transmittance over one ground-instantaneous-field-of-view (GIFOV) element, it determines the gain for one MISR pixel for each of thirty-six channels. Using a relative-response model of the array, this determination is used to derive an estimate of the array-averaged response. We combine this with the measure of the average gain as determined from OBC data using the equations

$$\overline{G}_1 = \frac{\sum(\overline{G}_{1,i}/\sigma_i^2)}{\sum(1/\sigma_i^2)}, \tag{10}$$

$$\sigma^2 = \frac{1}{N}\sum\sigma_i^2, \tag{11}$$

where i is the summation index over methodologies (in this case 2), $\overline{G}_{1,i}$ is the channel-average gain coefficient, and $\overline{G}_1$ is the combined channel-average gain coefficient. Let us assume we have six OBC observations and one vicarious observation which we believe to be accurate to the budgets given in Table 5. For a D camera, we believe our final calibration will have an uncertainty of 3.2 %; and for the A camera, 2.8 %. (D refers to a lens design that is used for the two most-oblique-viewing cameras; A refers to a lens design that is used for the nadir and two near-nadir viewing cameras.) A simple average of the uncertainties is taken, as these uncertainties are dominated by the systematic errors and do not decrease with the number of observations.

4. Aerosol retrieval over dark water

One way in which the MISR team is planning to take advantage of the care given to calibration is by incorporating instrument uncertainties directly into

the retrieval of geophysical quantities. We use the statistical formalism of chi-squared tests. In our aerosol retrievals, for example, we compare the measured radiances with model radiances, calculated for a range of possible aerosol amounts, compositions and size distributions. In the χ^2 tests, if the difference between the measured radiances and a comparison model are comparable with the instrument uncertainty, agreement between the model and the observation is judged to be significant. Absolute, camera-to-camera and band-to-band instrument uncertainties are automatically read from the radiometric calibration files into the MISR retrieval algorithm and are used in calculating the χ^2 test variables. Examples of this procedure can be found in land-surface, cloud and aerosol retrieval algorithms. One specific example is described here.

The MISR approach to retrieving aerosol over dark water is described in [7] and [12]. The algorithm compares top-of-the-atmosphere (TOA) measured reflectances with those computed from a model atmosphere. Each model atmosphere, in turn, is computed by varying the aerosol optical depth, effective particle radius, and the real and imaginary indices of refraction. Four specific tests are used to decide whether a comparison model is consistent with the measurements. Each test is based on the χ^2 statistical formalism [13].

The first criterion to be used to find the best-fitting optical depth is minimization of the reduced $\chi^2_{\rm abs}$ parameter, calculated as a function of optical depth as follows:

$$\chi^2_{\rm abs} = \frac{\sum_{\lambda=3}^{4}\left\{\sum_{j=1}^{9} w_j \cdot \frac{\left[\rho_{\rm MISR}(\lambda,j) - \rho_{\rm model}(\lambda,j)\right]^2}{\sigma^2_{\rm abs}(\lambda,j)}\right\}}{\sum_{\lambda=3}^{4}\left(\sum_{j=1}^{9} w_j\right)}, \tag{12}$$

where $\rho_{\rm MISR}(\lambda,j)$ is the MISR equivalent reflectance for band λ and camera j, computed by taking the median over the sub-regions in the 17.6 km $\times$ 17.6 km region which passed through all screens, $\rho_{\rm model}$ are the model TOA equivalent reflectances for the aerosol mixture, and $\sigma_{\rm abs}$ is the absolute radiometric uncertainty in $\rho_{\rm MISR}$. The sum over j corresponds to the cameras and the sum over λ corresponds to wavelength, and for dark water includes only Bands 3 and 4, the wavelengths at which the dark-water surface is assumed to have negligible reflectance. Equation (12) also contains weighting factors, w_j. For the dark-water retrievals, w_j is the inverse of the cosine of the view angle of camera j, providing a greater weighting to data from the more oblique cameras to take advantage of the longer atmospheric slant path.

The value of $\sigma_{\rm abs}$ is obtained by using calibration uncertainty information provided in the MISR ARP. To calculate $\sigma_{\rm abs}$ corresponding to equivalent reflectance $\rho_{\rm MISR}$, we first linearly interpolate the tabulated values of $\varepsilon_{\rm abs\_sys}$ and $\mathrm{SNR}_{4\times4}$ to this equivalent reflectance. Denoting these interpolated values $\varepsilon_{\rm abs\_sys}(\rho_{\rm MISR})$ and $\mathrm{SNR}_{4\times4}(\rho_{\rm MISR})$, we then have

$$\sigma^2_{\rm abs} = \rho^2_{\rm MISR}\left\{\left[\frac{\varepsilon_{\rm abs\_sys}(\rho_{\rm MISR})}{100}\right]^2 + \left[\frac{1}{\mathrm{SNR}_{4\times4}(\rho_{\rm MISR})}\right]^2\right\}. \tag{13}$$

Once $\chi^2_{\rm abs}$ has been minimized, its absolute value establishes whether or not the candidate aerosol model provides a good fit to the measurements. In theory, a value of $\chi^2 \leq 1$ indicates a good fit. However, to allow for unmodelled sources of uncertainty a value of $\chi^2 \leq 2$ is defined as an acceptable fit.

The second test makes use of the angular shape normalized to a reference camera (refcam), which emphasizes camera-to-camera geometric differences:

$$\chi^2_{\rm geom} = \frac{\sum_{\lambda=3}^{4}\left[\sum_{j=1}^{8} w_j \cdot \frac{\left[\frac{\rho_{\rm MISR}(\lambda,j)}{\rho_{\rm MISR}(\lambda,\mathrm{refcam})} - \frac{\rho_{\rm model}(\lambda,j)}{\rho_{\rm model}(\lambda,\mathrm{refcam})}\right]^2}{\sigma^2_{\rm geom}(\lambda,j)}\right]}{\sum_{\lambda=3}^{4}\left[\sum_{j=1}^{8} w_j\right]}, \tag{14}$$

where $\sigma_{\rm geom}$ (a dimensionless quantity) is the uncertainty in the measured camera-to-camera equivalent-reflectance ratio, given by

$$\sigma^2_{\rm geom}(\lambda,j) = \frac{\sigma^2_{\rm cam}(\lambda,j)}{\rho^2_{\rm MISR}(\lambda,\mathrm{refcam})} + \frac{\rho^2_{\rm MISR}(\lambda,j)}{\rho^2_{\rm MISR}(\lambda,\mathrm{refcam})} \cdot \frac{\sigma^2_{\rm cam}(\lambda,\mathrm{refcam})}{\rho^2_{\rm MISR}(\lambda,\mathrm{refcam})}, \tag{15}$$

in which $\sigma_{\rm cam}$ is the relative camera-to-camera calibration uncertainty in the equivalent reflectance $\rho_{\rm MISR}$. Equation (15) is derived by propagating the instrument errors [13]. The summation over cameras j excludes camera refcam. This reference camera is preferentially the nadir (An). For dark water, the summation over λ in (14) includes only Bands 3 and 4.

The value of $\sigma_{\rm cam}$ is obtained by using calibration-uncertainty information provided in the MSIR ARP. To calculate $\sigma_{\rm cam}$ corresponding to equivalent reflectance

ρ_{MISR} we again interpolate linearly. This is now done to obtain the values $\varepsilon_{\mathrm{cam\_sys}}$ and $\mathrm{SNR}_{4\times4}$ at this equivalent reflectance. Denoting these interpolated values $\varepsilon_{\mathrm{cam_sys}}(\rho_{\mathrm{MISR}})$and $\mathrm{SNR}_{4\times4}(\rho_{\mathrm{MISR}})$, we then have

$$\sigma^2_{\mathrm{cam}} = \rho^2_{\mathrm{MISR}} \left\{ \left[\frac{\varepsilon_{\mathrm{cam-sys}}(\rho_{\mathrm{MISR}})}{100} \right]^2 + \left[\frac{1}{\mathrm{SNR}_{4\times4}(\rho_{\mathrm{MISR}})} \right]^2 \right\}. \quad (16)$$

Two other goodness-of-fit parameters are the angular shape of the spectral ratio relative to Band 3, χ^2_{spec}, and a maximum deviation parameter, $\chi^2_{\mathrm{max\,dev}}$, or the channel at which the observed equivalent reflectance differs most from the model equivalent reflectance.

Successful aerosol models are those for which all four values, χ^2_{abs}, χ^2_{geom}, χ^2_{spec} and $\chi^2_{\mathrm{max\,dev}}$ are less than, or equal to, the threshold value of 2. This threshold value may be adjusted pending further studies of the theoretical sensitivity and experience with actual MISR data.

Acknowledgements. The work described in this paper is being carried out by the Jet Propulsion Laboratory, California Institute of Technology, under contract with the National Aeronautics and Space Administration.

References

1. Diner D., Beckert J., Reilly T., Ackerman T., Bruegge C., Conel J., Davies R., Gerstl S., Gordon H., Kahn R., Martonchik J., Muller J.-P., Myneni R., Pinty B., Sellers P., Verstraete M., Multi-angle Imaging SpectroRadiometer instrument description and experiment overview, *IEEE Trans. Geosci. Remote Sensing*, 1998, **36(4)**, 1072-1087.
2. Bruegge C. J., Duval V. G., Chrien N. L., Korechoff R. P., Gaitley B. J., Hochberg E. B., MISR prelaunch instrument calibration and characterization results, *IEEE Trans. Geosci. Remote Sensing*, 1998, **36(4)**, 1186-1198.
3. Bruegge C. J., Duval V. G., Chrien N. L., Diner D. J., Calibration Plans for the Multi-angle Imaging SpectroRadiometer (MSIR), *Metrologia*, 1993, **30**, 213-221.
4. Fox N. P., Martin J. E., *Appl. Opt.*, 1990, **29**, 4686-4692.
5. Geist J., Zalewski E. F., Schaefer A. R., *Appl. Opt.*, 1980, **19**, 3795.
6. Woodhouse R. M., Bruegge C. J., Gaitley B. J., Saghri G., Chrien N., Multi-angle Imaging SpectroRadiometer (MISR) Ancillary Radiometric Product (ARP), in *Earth Observing System II, Proc. SPIE*, 1997, **3117**.
7. Martonchik J. V., Diner D. J., Kahn R., Ackerman T. P., Verstraete M. M., Pinty B., Gordon H. R., Techniques for the retrieval of aerosol properties over land and ocean using multi-angle imaging, *IEEE Trans. Geosci. Remote Sensing*, 1998, **36(4)**, 1212-1227.
8. Martonchik J. V., Diner D. J., Pinty B., Verstraete M. M., Myneni R. B., Knyazikhin Yu., Gordon H. R., Determination of land and ocean reflective, radiative, and biophysical properties using multi-angle imaging, *IEEE Trans. Geosci. Remote Sensing*, 1998, **36(4)**, 1266-1281.
9. Taylor B. N., Kuyatt C. E., *Guidelines for Evaluating the Uncertainty of NIST Measurement Results*, NIST Technical Note 1297, 1994.
10. Chrien N. C. L., Bruegge C. J., Barkstrom B. R., Estimation of calibration uncertainties for the Multi-angle Imaging SpectroRadiometer (MSIR) via fidelity intervals., in *Sensor Systems for the Early Earth Observing System Platforms, Proc. SPIE*, 1993, **1939**, 114-125.
11. Diner D. J., Barge L. M., Bruegge C. J., Chrien T. G., Conel J. E., Eastwood M. L., Garcia J. D., Hernandez M. A., Kurzweil C. G., Ledeboer W. C., Pignatano N. D., Sarture C. M., Smith B. G., The Airborne Multi-angle SpectroRadiometer (AirMSIR): instrument description and first results, *IEEE Trans. Geosci. Remote Sensing*, 1998, **36(4)**, 1339-1349.
12. Diner D. J., Abdou W. A., Ackerman T. P., Crean K., Gordon H. R., Kahn R. A., Martonchik J. V., McMuldroch S. R., Paradise S. R., Pinty B., Verstraete M. M., Wang M., West R. A., *Level 2 Aerosol Retrieval Algorithm Theoretical Basis*, Jet Propulsion Laboratory Internal Document JPL D-11400, Rev C.
13. Bevington P. R., Robinson D. K., *Data Reduction and Error Analysis for the Physical Sciences*, 2nd ed., New York, McGraw Hill, Inc., 1996.